Prediction of inter-particle adhesion force from surface energy and surface roughness

Journal Item

VSP
Journal of Adhesion Science and Technology 0 (2010) 1–18
Journal of ADHESION SCIENCE and TECHNOLOGY
brill.nl/jast

Prediction of Inter-particle Adhesion Force from Surface Energy and Surface Roughness

Laila J. Jallo [a], **Yuhua Chen** [a], **James Bowen** [b], **Frank Etzler** [c] **and Rajesh Dave** [a,*]

[a] New Jersey Center for Engineered Particulates, New Jersey Institute of Technology, 138 Warren Street, Newark, NJ, 07102-1982, USA

[b] Department of Chemical Engineering, The University of Birmingham, Edgbaston, Birmingham, B15 2TT, UK

[c] Boeringer-Ingleheim Pharmaceuticals, Inc., 900 Ridgebury Road, Ridgefield, CT 06877, USA

Abstract

Fine powder flow is a topic of great interest to industry, in particular for the pharmaceutical industry; a major concern being their poor flow behavior due to high cohesion. In this study, cohesion reduction, produced *via* surface modification, at the particle scale as well as bulk scale is addressed. The adhesion force model of Derjaguin–Muller–Toporov (DMT) was utilized to quantify the inter-particle adhesion force of both pure and surface modified fine aluminum powders (∼8 μm in size). Inverse Gas Chromatography (IGC) was utilized for the determination of surface energy of the samples, and Atomic Force Microscopy (AFM) was utilized to evaluate surface roughness of the powders. Surface modification of the original aluminum powders was done for the purpose of reduction in cohesiveness and improvement in flowability, employing either silane surface treatment or dry mechanical coating of nano-particles on the surface of original powders. For selected samples, the AFM was utilized for direct evaluation of the particle pull-off force. The results indicated that surface modification reduced the surface energy and altered the surface nano-roughness, resulting in drastic reduction of the inter-particle adhesion force. The particle bond number values were computed based on either the inter-particle adhesion force from the DMT model or the inter-particle pull-off force obtained from direct AFM measurements. Surface modification resulted in two to three fold reductions in the Bond number. In order to examine the influence of the particle scale property such as the Bond number on the bulk-scale flow characterization, Angle of Repose (AOR) measurements were done and showed good qualitative agreements with the Bond number and acid/base surface characteristics of the powders. The results indicate a promising method that may be used to predict flow behavior of original (cohesive) and surface modified (previously cohesive) powders utilizing very small samples, and that the surface modification can drastically improve the powder flow for industrially relevant materials.

Keywords

Inverse gas chromatography, surface energy, inter-particle adhesion force, bond number, acidity and basicity, powder flow, cohesion reduction, surface modification

* To whom correspondence should be addressed. Tel.: +1 973 596 5860; e-mail: dave@adm.njit.edu

DOI:10.1163/016942410X525623

1. Introduction

Fine particles, of less than 30 μm in size, have attracted academic and industrial interest for over 50 years due, in part, to their high specific surface area. Fine powders are widely employed in several areas including, for instance, the chemical, energy, pharmaceutical, cosmetic and food industries. Fine aluminum powder ($<$10 μm) is used as an additive in energetic materials and as a fuel for various applications, due to its high calorific value [1–4]. Such powders, however, have very high tendency to agglomerate before and during combustion due to the presence of high surface forces, and they show poor flowability due to cohesion forces arising mainly as a result of van der Waals forces [5] that dominate over gravitational forces [6]. In order to improve the flow of such fine aluminum powders as well as to reduce their agglomeration in the combustion chamber, various approaches have been developed, e.g., encapsulating the aluminum particles with organic or inorganic materials [7, 8]. The poor flowability of the aluminum powder, that is studied here, is an illustrative example of powder flow problems observed in the pharmaceutical, chemical and food industries.

For aluminum powders as well as powders used in other industries where wet-processing based encapsulation is not feasible, dry coating technique [9] may also be used to improve flowability, reduce agglomeration, and improve processing of otherwise cohesive powders. Dry coating has been shown to be efficient in reducing the interparticle adhesion forces for not only improving the flowability [10] but also fluidizabilty [11] of fine powders by precisely depositing small amounts of nano-sized particles (called guest particles) on the surface of primarily cohesive powders (or host material). The deposits artificially generate nanoscale roughness, which can reduce the area of contact when two surfaces are in touch with each other. Yang *et al.* [10] found that the adhesion force between dry coated fine particles reduced in proportion to the ratio of the guest particle radius to the average asperity radius of the host particle, and is a major factor that contributes to the flow improvement.

While fine particles have high utility in diverse application domains, the particle cohesiveness is difficult to control, alter, measure and model since it is influenced by numerous factors, e.g., particle size/size distribution, particle shape, surface roughness, surface energy, material properties that include hardness, elasticity, deformation and even interstitial air. It is desirable to develop a reliable, simple strategy to evaluate particle-scale cohesiveness utilizing small powder samples with an objective to correlate such measurements with bulk-scale flowability. Towards that objective, indirect and direct measurements of adhesion forces of pharmaceutical powders have been performed [12]. Using particle interaction theories and AFM, indirect and direct adhesion forces could respectively be quantified. According to Johnson *et al.* [13] and Derjaguin *et al.* [14], the adhesion force of large, smooth, spherical particles undergoing elastic deformation is directly proportional to the work of adhesion and the particle size. The particle size is a good indicator of the level of adhesion that can be expected. In particular, the Bond number, which is defined as the ratio of cohesion force to the particle weight, relates inversely to the

powder flowbility, and also relates inversely to powder size, and thus powder size and powder flowability are strongly related. However, for particles with rough surfaces within the same size range, the particle size can be replaced by the surface roughness in estimating the influence of the adhesion force because real contact occurs only at the tips of the surface asperities [15]. It is emphasized that the particle size, which is part of the Bond number calculation, is still the dominant factor; however, the surface roughness has a significant effect on the adhesion force of up to orders of magnitude [16–18]. For particles of diameter 10–100 μm, it has been shown that the measured adhesion force is smaller than the theoretical due to reduction in contact area as a result of surface roughness [19, 20]. Surface roughness is obtained from topographical AFM scan which is described by the average height of the asperities, the standard deviation of the asperity height, and the fractional coverage of the surface by the asperities. Work of adhesion, which is related to surface energy, is typically obtained from IGC.

IGC has been used to analyze the surface energy of alumina [21], silica [22–24], carbon [25], etc. It is based on the physical adsorption of gaseous probes on the solid surface. From the elution peak, the retention time is obtained and is used to calculate the retention volume which, in turn, allows the surface energy of the material to be calculated. The surface energy is considered to result from two components: a Lifshitz–van der Waals (LW) dispersion component and an acid–base component. IGC will employ methods proposed by Gray [26, 27] and Papirer [28] for the determination of the dispersion and acid–base components, respectively.

The objective of this study was to alter the inter-particle adhesion force of aluminum powder using surface modification (introducing nano-roughness) and measure inter-particle adhesion both directly using AFM and indirectly using both IGC and particle topography by AFM. A new way of quantifying particle adhesion is being proposed in which the adhesion force could be correlated to angle of repose.

1.1. Particle Adhesion Theory

Solid–solid interaction is a short range phenomenon with characteristic length defined by the equilibrium inter-atomic distance z, and follows the force law derived from the Lennard–Jones potential:

$$p_{a(z)} = \frac{8\omega}{3z_0}\left[\left(\frac{z}{z_0}\right)^{-9} - \left(\frac{z}{z_0}\right)^{-3}\right]. \quad (1)$$

Here z_0 is the equilibrium separation distance, ω is the work of adhesion, usually denoted by surface free energies as $\omega = \gamma_1 + \gamma_2 - \gamma_{12}$ where γ_1 and γ_2 are the surface free energies of the two interacting solid surfaces and γ_{12} is the interfacial energy at the solid–solid interface, and p_a is the compressive positive force. Two solids in molecular or intimate contact exhibit adhesion interaction which can be

modeled by the JKR [13] or the DMT [14] models. Tabor [29] pointed out that these two theories applied to opposite extremes of a spectrum of the parameter

$$\mu_T = \left(\frac{16R\omega^2}{9K^2 z_0^3}\right)^{1/3}, \tag{2}$$

where for the same contacting materials $\omega = 2\gamma$, and $K = \frac{2}{3}[\frac{E}{(1-\nu)}]$. Here R is the radius of curvature (in this case considered to be the asperity on the surface of the particles), E is the elastic modulus, ν is Poisson ratio, z_0 is the inter-atomic equilibrium distance in the Lennard–Jones potential for solid–solid interaction, γ is the LW component of surface energy and ω is the adhesion energy or work of adhesion. The parameter μ_T represents the ratio of the displacement of the surfaces at the point of separation within the effective range of surface forces. In the DMT zone of the spectrum, elastic deformation due to surface forces is negligible, whereas in the JKR zone of the spectrum, elastic deformation effects are significant [30].

Muller *et al.* [31], showed that μ_T varies with the pull-off force from $\mu_T < 0.1$ for the DMT model to $\mu_T > 5$ for the JKR model. The DMT model has been found to be valid for small particles, small surface energy, and high elastic modulus and the converse is true for the JKR model. In the two models the relationship between the force of adhesion and the adhesion energy is given by $F_{\text{ad}} = n\pi R^*\omega$. Where n is 3/2 for the JKR model and 2 for the DMT model, and R^* is the contact radius.

In this work, the DMT model was employed to predict the LW dispersion force. The characteristic radius of the root-mean-square value of surface roughness measurement was used as the estimate for the contact radius R^*, and the value of the LW dispersion component of surface energy measured from IGC was used to obtain the work of adhesion. In addition, the acid–base interactions were obtained using the topological indices of the probes.

2. Materials and Methods

2.1. Materials

All aluminum powders were supplied by the Naval Air Warfare Center, China Lake, California. The hydrophobic silica (R972) was obtained from Degussa, USA. All of the chromatographic-grade probes were purchased from Sigma Aldrich, USA. Cornstarch was purchased from Argo, USA. Properties of the materials used are summarized in Table 1.

Sample denoted by A1 is the raw material, samples A2 to A6 are surface modified powders with silane and A7 is the nano-silica coated sample. The methods used for surface modification were dry particle coating for A7 and silane treatment of the surface of the aluminum particles for samples A2–A6. These methods have been extensively discussed in detail in [9, 10] for dry coating and [32] for silane treated materials. The silane used in this work was methyltrichlorosilane (CH_3SiCl_3) purchased from Sigma-Aldrich USA. One or two successive coatings

Table 1.
Physical properties of the aluminum powders used

Sample	Surface treatment	Mean particle size (μm)	D10 (μm)	D50 (μm)	D90 (μm)	LW dispersion component of surface energy (mJ/m^2)	Work of adhesion (mJ/m^2)	R_{rms} surface roughness (nm)	Standard deviation of roughness (nm)
A1	None	9.4	5.1	8.4	14.7	123.0	246	16.7	11.2
A2	Silane	9.7	5.5	8.8	14.2	19.9	39.8	4.7	3.3
A3	Silane	8.2	4.1	7.9	13.1	28.8	57.6	10.2	2.9
A4	Silane	9.2	4.6	8.6	14.3	23.0	46.0	9.6	4.4
A5	Silane	9.1	4.2	7.9	14.8	30.9	61.8	8.8	3.7
A6	Silane	8.7	3.7	7.5	13.9	31.4	62.8	8.1	3.2
A7	Nano-silica	8.7	4.6	8.0	13.9	26.7*	53.4*	17.1	11.7

* Surface energy and work of adhesion of nano-silica (R972) respectively.

of silane at different experimental conditions were applied to cover the surface of the aluminum particles. The basic procedure involved mixing of aluminum powder with silane solution in hexane. The process was carried out in a stainless steel kettle with a stirrer that ensured thorough mixing of the solution of silane and aluminum powders. After mixing, hexane was evaporated through gentle water jacket based heating and the treated aluminum powder was sieved to obtain the final product. This is a wet process requiring substantial amounts of organic solvent, in particular when multiple passes are employed.

2.2. SEM Images

Images showing the particle morphology, the presence of guest particles on the surface of dry-coated host particles, the roughness of the surfaces of the uncoated and silane treated particles, and morphology of the agglomerates of the original material were obtained with a LEO 1530VP Field Emission Scanning Electron Microscope (FESEM). For the purpose of FESEM imaging, powder samples were mounted on aluminum stubs using a double-sided adhesive carbon tape and were sputter coated with carbon.

2.3. AFM Topographical Images

Topographical images of the surface of the particles were obtained with a MultiMode AFM with a Nanoscope III controller (Digital Instruments, USA) in the tapping mode using a silicon probe purchased from Veeco, USA. The particles were mounted on a silicon wafer using a double-sided adhesive carbon tape. The root-mean-square surface roughness was obtained from the deviations from average height data over a 500 nm × 500 nm area.

2.4. AFM Inter-particle Force Measurement

Adhesion force measurements were performed using a MultiMode AFM with a Nanoscope IIIa controller (Digital Instruments, USA) under ambient conditions at a relative humidity of 50–60%. The procedure involved mounting the aluminum particles onto a cantilever and a substrate using cyanoacrylate glue. The cantilever is approached and retracted from the substrate as described in [33]. By applying Hooke's Law, $F = kx$, where x is the deflection of the cantilever and k is the spring constant of the cantilever, the adhesion force can be calculated.

2.5. Flow Characterization

A Hosokawa Powder Tester model PT-N was used to measure the angle of repose (AOR). The procedure used to measure AOR was as per ASTM D6393-99 standard "Bulk Solids Characterization by Carr Indices", and each reading was an average of three observations. To measure the AOR, the powder was placed in the powder holder in the device. The equipment was then set to run for 180 s and a suitable vibration rate depending on the powder was chosen. At the end of the run the measuring pin was aligned parallel to the slanting surface of the powder and the resulting angle obtained was recorded.

2.6. Inverse Gas Chromatography

Inverse gas chromatography (IGC) at infinite dilution was used to obtain the surface energy of the powders. The measurements were done with a Gas Chromatograph (Varian 3600) with a Flame Ionization Detector (FID). All measurements were done at 40°C column temperature.

Stainless steel columns of 5 ft length and 2.16 mm diameters were packed with approximately 5.0 g of the powder by Restek, Bellefonte, PA, USA. The columns were conditioned for 24 h with helium at a flow rate of approximately 20 ml/min and temperature of 250°C to remove moisture and impurities. The retention times of methane, a series of n-alkanes (pentane to octane), and polar probes (dichloromethane (DCM), diethylether (DEE), tetrahydrofuran (THF) and chloroform) were obtained from the elution peaks in the chromatogram at infinite dilution. The net retention volume is calculated from the measured retention time [34] and the LW dispersion component of the surface energy γ_s^d is calculated from the relationship [35]:

$$\gamma_s^d = \frac{1}{4\gamma_{CH_2}}\left[\frac{\Delta G_a^{CH_2}}{N a_{CH_2}}\right]^2. \quad (3)$$

In this expression, the only unknown is γ_s^d. Here, γ_{CH_2} is the surface energy of a molecule with a CH_2 group, given by $\gamma_{CH_2} = 36.8 - 0.058T$ (°C); N is Avogadro's number; a is the area of an adsorbed –CH_2-group given as 6 Å^2 and $\Delta G_a^{CH_2}$ is the slope of Fig. 1.

The electron donor and acceptor properties were determined using the approach by Brendle and Papirer [28], which relies on the topological indices of the probes.

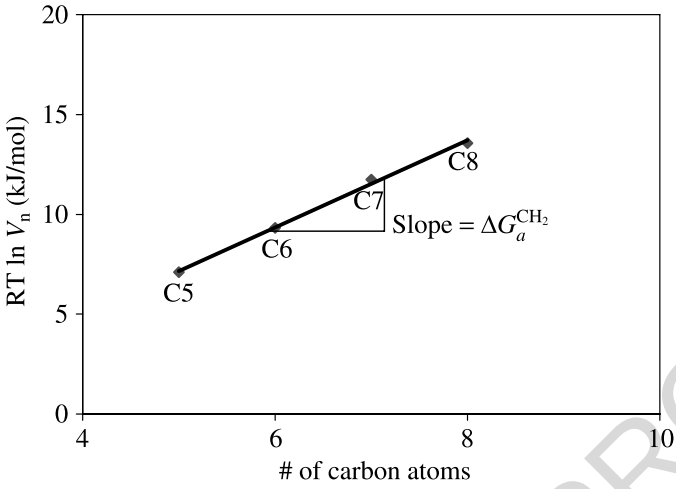

Figure 1. Plot of variation of RT ln V_n with number of carbon atoms of linear alkane probes.

They determined the indices based on the work of Barysz *et al.* [36], which is an extension of the Wiener index. This approach [36] first requires the formation of a graph and the determination of the matrix distance of the probe molecule. For example, the graph of pentane will result in a 5×5 distance matrix and that of chloroform will result in a 4×4 distance matrix.

Then the weighted values of the elements of the distance matrix are calculated from the atomic numbers of the elements which make up the molecule.

For the elements in the diagonal, the weight is calculated from

$$d_{ii} = 1 - \frac{6}{Z_i}, \tag{4}$$

where Z_i is the number of electrons of atom i.

For all other elements in the matrix

$$d_{ij} = \sum k_r, \tag{5}$$

$$k_r = \frac{1}{b_r} \times \frac{36}{Z_{i'} \cdot Z_{j'}}, \tag{6}$$

where b_r is 1, 2 or 3 if the bond between the atoms is single, double or triple respectively, and Z_i and Z_j are the total number of electrons of the atoms i and j forming the bond.

The Wiener index W, is then calculated from

$$W = \frac{1}{2} \sum_{i=1}^{n} d_{ii} + \frac{1}{2} \sum_{i=1}^{n} \sum_{j=1}^{n} d_{ij} \tag{7}$$

and the topological index is then evaluated from

$$\chi_\tau(W) = 1.8789 \times W^{0.3271}. \tag{8}$$

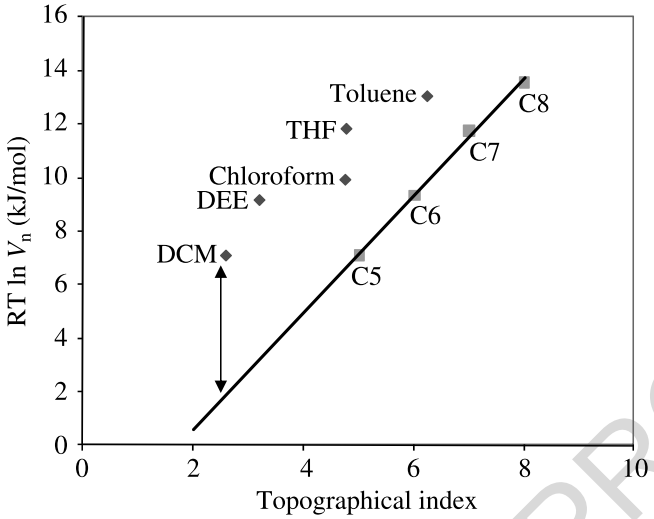

Figure 2. Plot of RT ln V_n with the topographical index of each probe. The *n*-alkanes fall on a straight line and all the polar probes fall to the left of the line. The free energy of specific interaction ΔG_{sp} is obtained from the difference between the *y*-value of the polar probe to the corresponding *y*-value on the *n*-alkane line. The polar probes are dichloromethane (DCM), diethylether (DEE), tetrahydrofuran (THF), and chloroform.

The specific interaction ΔG_{sp} is related to the acidity (K_a) and basicity (K_d) by the following equation:

$$\frac{\Delta G_{sp}}{AN^*} = \left(\frac{DN}{AN^*}\right) K_a + K_d, \tag{9}$$

where AN^* and DN are the electron acceptor and electron donor numbers, respectively, characterized according to Gutmann [37]. The values of K_a and K_d were obtained from the slope and intercept, respectively, of the plot of equation (9).

3. Results and Discussion

3.1. SEM Images

The representative SEM images shown in Fig. 3 are those of as-recieved (a), silica coated (b), silane treated (c) and particle shape and agglomerates formed of as-recieved sample (d) of aluminum particles. The silane treated and silica coated powders are based on the modification of as-recieved aluminum powder (a), and all are mostly spherical in shape as shown in (d). The surface asperities, as shown in images (a), (b) and (c) are distinctly different from each other. The naturally occurring surface asperity of the as-recieved aluminum powder in image (a) shows relatively large spacing between the sharp surface features. The asperities in images (b) and (c) are the result of surface modification, which show relatively smooth surface of silane treated particles and surface smoothness of dry coated particles due

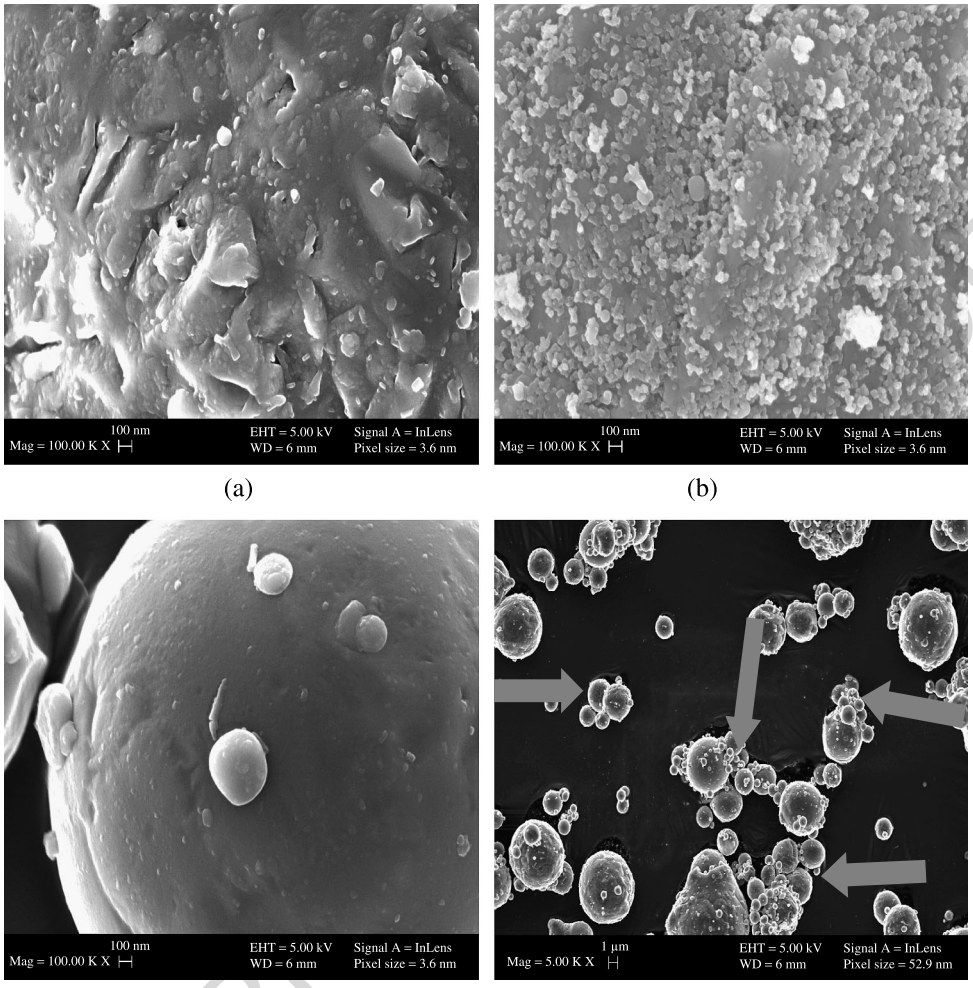

Figure 3. SEM images of (a) as-received aluminum particles, showing surface asperities, (b) surface asperities of silica coated particles (c) surface features of silane treated particles, and (d) morphology and agglomerates of as-received particles.

to the nano-sized particles filling the sharp features in (a). The magnitude of the surface asperity will either increase or decrease the adhesion force depending on the true contact area between the particles. Images (b) and (c) also show the coating density and uniformity on the surface. The aim of the surface modification of the particles is to increase nano-roughness and reduce adhesion force as a result of the reduction in true area of contact.

3.2. Flow Characterization

The angle of repose measurements in Fig. 4 show a trend of decreasing cohesiveness from the as-recieved aluminum powder (A1) through the dry coated sample (A7) to

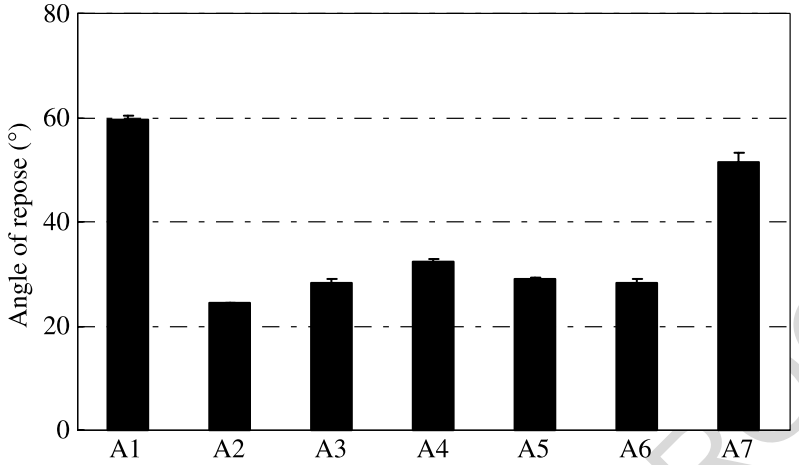

Figure 4. The angle of repose (AOR) of each of the powders. The smaller the AOR value is, the better the flowability.

the silane treated materials (A2–A6). The results show a clear distinction between the as-recieved, dry coated and silane treated powders, however, do not clearly distinguish the differences between some of the silane treated powders (A3, A5 and A6). As expected, the original powder is very cohesive, and yields the largest AOR value as compared to all the surface modified materials. The dry coated sample shows flow improvement as compared to the as-recieved, untreated powder, however, the silane treated powders gave the best flow results with a drastic decrease in cohesiveness.

3.3. Cohesiveness Characterization

Surface roughness values obtained from AFM topographical images are presented in Table 1. The untreated material (A1) and dry coated sample (A7) have relatively rough surfaces as compared to the silane treated materials, with mean roughnesses of 16.7 nm, 17.1 nm and standard deviations of 11.2 nm, 11.7 nm respectively. The dry coated sample has asperity size comparable to the size of the nano-silica used in the surface modification. The silane treated samples A2 through A6 have smoother surfaces with mean roughness values ranging from 4.7 nm to 10.2 nm and standard deviations ranging from 2.9 nm to 4.4 nm. The surface roughness of samples A2 through A6 seems to depend on the conditions under which the surface silanization was done. For instance, A2 has the smallest roughness (4.7 nm with standard deviation 3.3 nm) and A3 has the largest roughness (10.2 nm with a standard deviation of 2.9 nm). For the case of the silane treated samples, the smoothness of the surface due to the silanization seems to imply more uniform coating and hence appears to be the determining factor in the surface energy values of the samples as shown in Table 1. In other words, improved smoothness correlates with lower surface energy. Sample A2 gave a significantly low surface energy and low surface roughness as compared to all the other silanized samples.

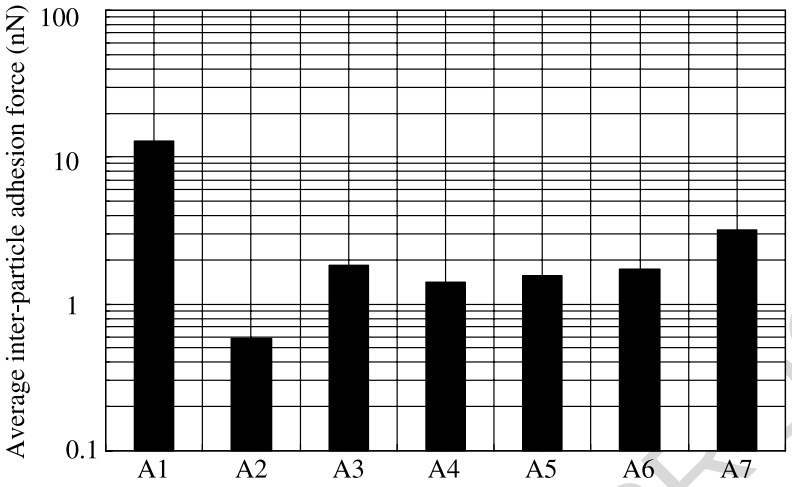

Figure 5. Predicted average inter-particle adhesion force for all samples calculated from the DMT model using measured surface energy and surface roughness values.

Table 2.
Values of adhesion and pull-off force of the aluminum and cornstarch particles calculated from the DMT-model and obtained experimentally from AFM, respectively

Sample	Adhesion force (nN), from DMT-model	Pull-off force (nN), from AFM		
		10 μm diameter	6 μm diameter	15 μm diameter
A1	12.9	47.3 ± 1.8	9.0 ± 0.3	–
A2	0.6	–	–	–
A3	1.8	–	–	–
A4	1.4	–	–	–
A5	1.7	–	–	–
A6	1.6	13.5 ± 2.3	8.1 ± 0.9	–
A7	3.2	15.3 ± 3.3	9.6 ± 2.0	–
Cornstarch + 0.5% R972	2.86	–	–	2.6 ± 0.8

In Fig. 5 and Table 2, the inter-particle adhesion force calculated from the dispersion component of surface energy and the surface roughness, using the DMT model, i.e., $F_{ad} = n\pi R^*\omega$ is presented for each powder sample. The results show a trend similar to that observed in the flow test results. The adhesion of the uncoated sample A1 is greater than that of all the surface modified materials. All the silane treated samples (A2–A6) have lower adhesion as compared to the silica coated (A7), and the untreated sample A1. From the plot, the adhesion can be grouped into 4 separate classes. The as-recieved, untreated material A1, the silica coated A7, silane treated A2, and silane treated A3, A4, A5 and A6. Two of the main factors influencing adhesion force between particles considered in this work are the geometry of contact

which is controlled by the surface roughness and the work of cohesion/adhesion. The relatively smooth surface shown in Fig. 3(c), which is representative of all the silane treated materials, has smaller asperity size and spacing as indicated by the R_{rms} values in Table 1 when compared to the uncoated and dry coated samples, shown in Fig. 3(a) and 3(b) respectively. These smaller asperity size and spacing correspond to lower adhesion force as shown in Fig. 5. Meanwhile, the dry particle coated sample having about the same asperity size and spacing as the uncoated sample also showed drastic decrease in adhesion force as compared to the uncoated sample. This result indicates somewhat surprising fact that although the visible surface roughnesses in Fig. 3(a) and 3(b) are very different, their R_{rms} values are very comparable. The fact is that the dry coated sample shows an improvement in the flowability as compared to untreated sample, and it appears that at this nano-scale surface roughness, the surface roughness may be playing only a minor role in adhesion reduction while the dominating factor is the surface energies of these samples. As the values in Table 1 show, the dispersion components of surface energies of all the surface modified materials are about one fourth of the uncoated material. Another observation that can be made is that the reduction in adhesion force for the dry coated sample A7 is significant as compared to the original material, A1 as seen in Fig. 5. However, the improvement in flowability as indicated by AOR as shown in Fig. 4 is not that significant. One possible reason is the reduction in the particle size (the volume average size decreased from 9.4 μm to 8.7 μm, and more significantly, the number average size decreased from 3.7 μm to 3.3 μm) that occurs due to attrition caused by the dry coating process. At such size scale, such reduction can lead to less than significant flowability improvement. The influence of the particle size is considered in more detail next.

In Table 2, in addition to the aluminum powders, a value for the cornstarch powder is also presented. As can be seen, the DMT as well as direct AFM measurements agree very well for the cornstarch powder, while they agree well within an order of magnitude for the aluminum powders.

To estimate the effect of particle size on the cohesiveness/flowability of the powders, the granular Bond number $\mathrm{Bo_g}$ is calculated from the adhesion forces in Fig. 5 and Table 2. As mentioned before, the Bond number is defined as the ratio of cohesion force to the particle weight. In order to estimate the Bond number, an average particle size is needed to estimate the particle weight; for this purpose, either the number averaged or volume averaged particle size may be used. Figure 6 shows comparison of the AOR with the Bond number of the powders; where in Fig. 6(a) the Bond number is derived from number average particle size and in Fig. 6(b), it is based on the volume average particle size. In both figures, all the measured data fit reasonably well to a logarithmic trend-line, and a one-to-one correspondence can be observed between the AOR and the Bond number values, indicating a good qualitative agreement between the particle-scale and bulk-scale metrics. Similar to that of Fig. 5, the samples are grouped into 4 distinct classes, with A1 (original untreated sample) having the highest Bond number and AOR value and A2 (the best silane

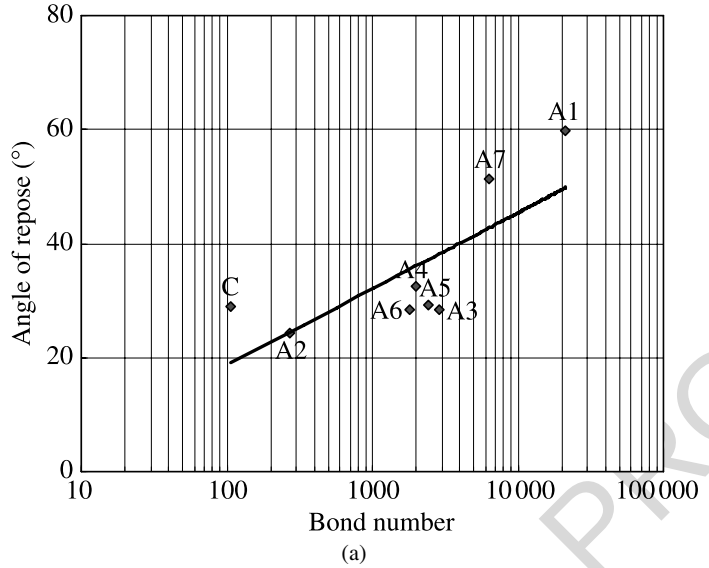

(a)

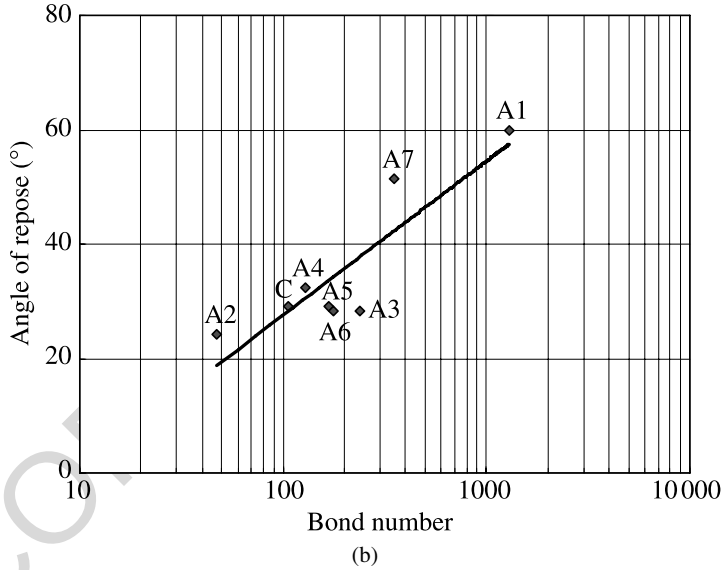

(b)

Figure 6. Angle of repose *vs*. granular bond number Bo_g for the samples listed in Table 1. The line is a logarithmic fit to the data. The Bond numbers were calculated from the adhesion force predicted from the DMT model. The Bond numbers in (a) were calculated from number average particle size and in (b) were calculated from volume average particle size. The letter C represents cornstarch dry coated with 0.5% silica (R972).

treated) having the least. The rest of the silane treated (A3–A6) and the dry coated (A7) samples fall in between A1 and A2, with the silane samples (A3–A6) grouped together at a lower Bond number and AOR than the dry coated sample (A7). These results show that a simple model like the DMT could be used to calculate the cohe-

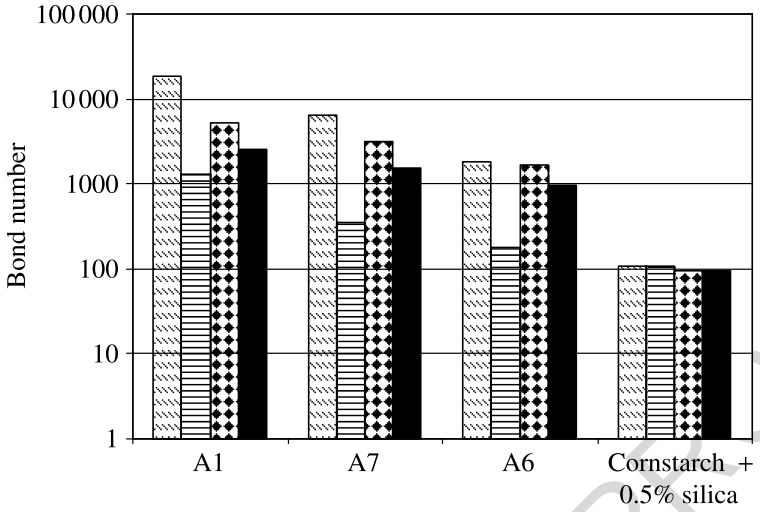

Figure 7. Plot of granular Bond number Bo_g for as-received (A1), silica coated (A7) and silane treated (A6) aluminium particles. The Bond numbers were calculated from both AFM pull-off force and adhesion force obtained from DMT model. For each powder sample, the first two bars are the Bond number values estimated based on number average and volume average particle sizes where the adhesion force was obtained from the DMT model, while the last two bars are direct AFM measurements of the adhesion force for two different particles in each case (for aluminium, the particle sizes were 6 μm and 9 μm, respectively, while both cornstarch particles were of the same size, 15 μm). (▨ Number average particle size of aluminum particles ∼4 μm (DMT), ▤ volume average particle size of aluminum particles ∼9 μm (DMT), ⊡ 6 μm aluminum particle (AFM), ■ 10 μm aluminum particle (AFM).)

siveness represented by the Bond number, and it can subsequently follow the same rank order as the bulk level flowability of surface modified powders.

While Fig. 6 employs the Bond numbers computed from the ensemble averaging done *via* the measurement of surface energy and the use of an average particle size, one could also directly employ AFM to measure inter-particle adhesion force to evaluate the Bond number for an individual particle. In Fig. 7, we present the comparison of the Bond numbers obtained from the direct AFM measurements from values of pull-off force in Table 2 with the DMT model for selected powder samples. For the AFM measurements, few individual particles of 6 μm and 10 μm sizes were selected. In addition to three aluminium powder samples, we have also included one result for cornstarch (supplied by Argo), having nominal size about 15 μm and coated with 0.5 wt% silica (R972). Cornstarch represents materials used in food and pharmaceutical industries. For cornstarch, the number and volume averaged particle sizes are nearly the same and two different size samples used for AFM analysis are also nearly the same. The figure shows the influence of particle size, surface modification and adhesion measurement method (direct AFM or DMT model). As discussed before, the Bond numbers for Fig. 6 are calculated from interparticle adhesion force obtained *via* DMT model and the estimate of average particle size. The bars in Fig. 7 show the results from Fig. 6 based on the average

particle size and adhesion force estimated from DMT model as well as the Bond numbers calculated from individual particle pull-off force obtained from AFM. The results show that an increase in particle size corresponds to a decrease in Bond number and that the surface modification leads to a decrease in Bond number which is more pronounced for the smaller size particle. This is in line with the observations reported in the literature [38, 39]. In case of cornstarch, since the particle size distribution is such that the number and volume averages particle sizes are similar, the DMT model based and AFM measurement based Bond number values are almost the same. Even for the case of aluminium powders the values are comparable. An important observation can be made from the results shown in Fig. 7 that the Bond numbers obtained from the direct AFM measurements are comparable to those obtained from the DMT model, in particular when the volume averaged size is used in estimating the DMT model based Bond number. This is a very useful observation since the procedure outlined for using the DMT model is more reliable than the direct AFM measurements where one must rely on the results based on a few selected particles and there are difficulties involved with mounting a particle on a cantilever and substrate and making sure the particles are properly aligned during the AFM measurements.

The variation in free energy of specific interaction reported in Table 3 shows that all powders interacted more strongly with the acidic probes (DCM and chloroform) than the basic probes (DEE, THF), except for the raw material A1, which shows about the same magnitude of interaction with both the acidic and the basic probes. A1, as expected, shows amphoteric behavior which is typical of alumina (the thin oxide layer on the surface of aluminum particles). For both acidic and basic probes there was a reduction in the free energy of specific interaction of all the surface modified powders as compared to the original as-recieved material A1. The strong interaction shown by all surface modified powders with the acidic probes is an indication that they behave like electron donors or Lewis base when interacting with other powders. Figure 8 shows a plot of AOR with the acid–base characteristic of the powders, denoted by the ratio of basicity to acidity. The plot follows the same trend as in Figs 5 and 6 in terms of near one-to-one correspondence between

Table 3.
Values of free energy of specific interaction (kJ/mol) of the polar probes with the aluminum powders. Dichloromethane (DCM), Diethyl ether (DEE) and Tetrahydrofuran (THF)

	Sample						
Probe	A1	A2	A3	A4	A5	A6	A7
DCM	10.67	2.79	6.33	5.90	6.80	6.57	5.84
DEE	10.50	0.58	1.94	0.71	2.51	1.34	0.87
THF	12.72	0.85	2.45	1.99	3.46	2.59	2.25
Chloroform	15.01	3.33	5.78	5.27	7.17	5.82	5.85

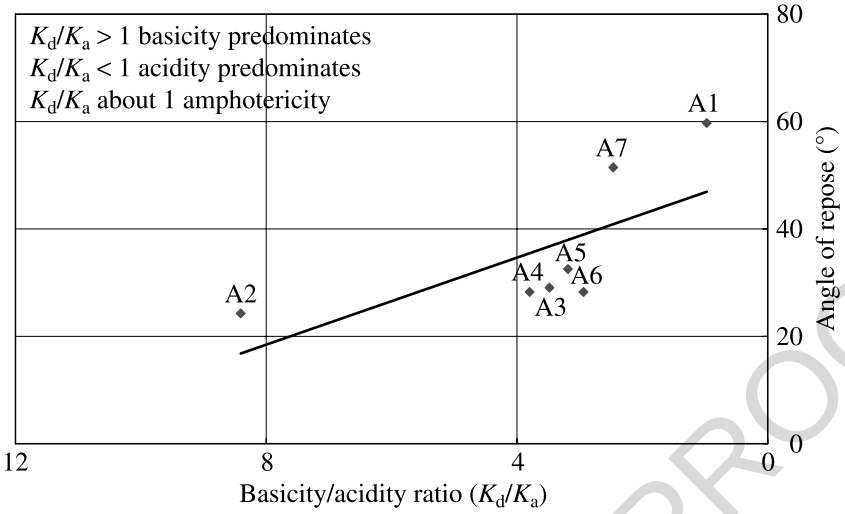

Figure 8. The relationship between the AOR and basicity/acidity ratio of the surface of the particles. The plot indicates that the more basic the surface of the aluminum powders, the lower the angle of repose which may correlate to better flowability. Note that the abscissa is plotted in a descending order so as to show the similarity with Fig. 6.

the AOR and the acid–base characteristic and the fact that these samples fall in four groups; A1, A2, A3–A6 and A7. It also shows that the more basic the particle surface is, the better is the flowability of the powder.

4. Summary and Conclusions

The evaluation of cohesiveness reduction, carried out *via* surface modification using two methods, was performed at particle-scale through indirect (DMT approach) as well as direct (AFM force evaluation) measurement of adhesion forces. The flowability of the original and surface modified powders was also evaluated at the bulk-scale using the Hosokawa Powder Tester in terms of the Angle of Repose. The results showed that surface modification can dramatically reduce the cohesiveness of the powders through the increase in flowabilty (reduced AOR) and reduction of adhesion force (reduced inter-particle adhesion force). The particle-scale adhesion was also presented in terms of the Bond number, which correlated well with the AOR values. With respect to the computation of the Bond number, the selection of the representative averaged value of the particle size becomes critical. As was shown, the numerical values of the Bond numbers will differ over an order of magnitude depending on which average diameter is taken, the number average or volume average. In contrast to the number average size that is biased towards fines, the volume average particle size better represents the average of the bulk of the powder. Therefore, it is suggested that the Bond number should be computed based on the volume average particle size. This value also agrees more closely with the direct AFM evaluation of the Bond number for 10 μm particles. The data for

dry-coated cornstarch powder show that results obtained from volume average and number average particle size follow the same trend in terms of the bulk-scale and particle-scale characterization and in addition, the Bond number estimation from the DMT model agrees with the AFM model. The results also show that the acid–base characteristics of these powders could be correlated to their flowabilty.

Overall, the results presented show that the use of DMT model could provide a predictive rank ordering of the surface modified powders because of the observed one-to-one correlation between the Bond number (particle-scale measure) and unconsolidated bulk-scale measure such as the AOR. Since there is an increased need for surface modified powders for the purpose of improved flow and other properties [9–12], it is advantageous to utilize this approach to evaluate the differences between powder batches or different surface modifications. This approach could also help evaluate Active Pharmaceutical Ingredient (API) powders during early drug development where the amount of sample available is very small and a decision needs to be made regarding the best alternative particle formation process, processing conditions, that can provide optimal flow characteristics.

Acknowledgements

Work at NJIT has been supported, in part, by the U.S. Navy Undersea Warfare Center and the National Science Foundation through the ERC (EEC-0540855) award. Authors also thank Aveka, Inc., Woodbury, MN, for providing the use of the MAIC device, Dr. Curtis E. Johnson, Naval Air Warfare Center, China Lake, California, USA for providing silane treated powders, and Ms. Lauren Beach for facilitating the AFM work performed at the University of Birmingham.

References

1. P. E. Pokhil, A. F. Belyaev, Y. V. Frolor, V. S. Logachev and A. I. Korotkov, *Combustion of Powdered Metals in Active Media*. Nauka, Moscow (1972).
2. K. K. Kuo and M. Summerfield (Eds), *Fundamentals of Solid Propellant Combustion*. AIAA, New York (1984).
3. A. P. Il'in, A. A. Gromov, V. I. Vereshchagin, E. M. Popenko, V. A. Surgin and H. Lehn, *Combustion, Explosion, and Shock Waves* **37**, 664–668 (2001).
4. Y. Kwon, A. A. Gromov, A. P. Ilyin, E. M. Popenko and G. Rim, *Combustion and Flame* **133**, 385–391 (2003).
5. J. Q. Feng and D. A. Hays, *Powder Technol.* **135–136**, 65–75 (2003).
6. A. B. Yu, C. L. Feng, R. P. Zou and R. Y. Yang, *Powder Technol.* **130**, 70–76 (2003).
7. A. P. Il'in, E. M. Popenko, A. A. Gromov, Y. Y. Shamina and D. V. Tikhonov, *Combustion, Explosion, and Shock Waves* **38**, 665–669 (2002).
8. O. G. Glotov, D. A. Yagodnikov, V. S. Vorob'ev, V. E. Zarko and V. N. Simonenko, *Combustion, Explosion, and Shock Waves* **43**, 320–333 (2007).
9. M. Ramkakhan, Y. Wu, S. Watano, R. N. Dave and R. Pfeffer, *Powder Technol*. **112(1–2)**, 137–148 (2000).
10. J. Yang, A. Sliva, A. Banerjee, R. Dave and R. Pfeffer, *Powder Technol*. **158**, 21–33 (2005).

11. Y. Chen, J. Yang, R. N. Dave and R. Pfeffer, *AIChE J.* **54**, 104–121 (2008).
12. D. Traini, P. Rogueda, P. Young and R. Price, *Pharmaceutical Res.* **22**, 816–825 (2005).
13. K. L. Johnson, K. Kendall and A. D. Roberts, *Proc. Roy. Soc. London Series A* **324**, 301–313 (1971).
14. B. V. Derjaguin, V. M. Muller and Y. P. Toporov, *J. Colloid Interface Sci.* **53**, 314–325 (1975).
15. K. L. Johnson, in: *Theoretical and Applied Mechanics*, W. T. Koiter (Ed.), pp. 133–143. North-Holland Publishing Company, Amsterdam (1976).
16. K. Cooper, A. Gupta and S. Beaudoin, *J. Electrochem. Soc.* **148**, G662 (2001).
17. K. Cooper, N. Ohler, A. Gupta and S. Beaudoin, *J. Colloid Interface Sci.* **222**, 63 (2000).
18. K. Cooper, A. Gupta and S. Beaudoin, *J. Colloid Interface Sci*. **228**, 213 (2000).
19. F. Podczeck and J. M. Newton, *J. Appl. Phys*. **79**, 1458–1463 (1996).
20. Y. I. Rabinovich, J. J. Adler, A. Ata, R. K. Singh and B. M. Moudgil, *J. Colloid Interface Sci*. **232**, 17–24 (2000).
21. E. Papirer, J. M. Perrin, B. Siffert, G. Philipponneau and J. M. Lamerant, *J. Colloid Interface Sci*. **156**, 104 (1993).
22. A. Vidal, E. Papirer, W. M. Jiao and J. B. Donnet, *Chromatographia* **23**, 121 (1987).
23. G. Ligner, A. Vidal, H. Balard and E. Papirer, *J. Colloid Interface Sci.* **133**, 200 (1989).
24. E. Papirer, H. Balard, Y. Rahmani, A. P. Legrand, L. Facchini and H. Hommel, *Chromatographia* **23**, 639 (1987).
25. J. Jagiello, T. J. Bandosz and J. A. Schwarz, *J. Colloid Interface Sci.* **151**, 433 (1992).
26. G. M. Dorris and D. G. Gray, *J. Colloid Interface Sci*. **77**, 353 (1980).
27. S. Katz and D. G. Gray, *J. Colloid Interface Sci*. **82**, 318 (1981).
28. E. Brendle and E. Papirer, *J. Colloid Interface Sci*. **194**, 217–224 (1997).
29. D. J. Tabor, *J. Colloid Interface Sci*. **58**, 1 (1976).
30. K. L. Johnson and J. A. Greenwood, *J. Colloid Interface Sci*. **192**, 326–333 (1997).
31. V. M. Muller, V. M. Yushenko and B. V. Deryaguin, *J. Colloid Interface Sci.* **77**, 91 (1980).
32. L. J. Jallo, M. Schoenitz, E. L. Dreizin, R. N. Dave and C. E. Johnson, *Powder Technology* (2010). In press.
33. M. Weth, M. Hofmann, J. Kuhn and J. Fricke, *J. Non-Crystalline Solids* **285**, 236–243 (2001).
34. M. M. Chehimi, M.-L. Abel, C. Perruchot, M. Delamar, S. F. Lascelles and S. P. Armes, *Synthetic Metals* **104**, 51–59 (1999).
35. A. Khalfi, E. Papirer, H. Balard, H. Barthel and M. G. Heinemann, *J. Colloid Interface Sci*. **184**, 586–593 (1996).
36. M. Barysz, G. Jashari, R. S. Lall, V. K. Srivastava and N. Trinajstic, *Stud. Phys. Theor. Chem.* **28**, 222 (1983).
37. V. Gutmann, *The Donor–Acceptor Approach to Molecular Interactions*. Plenum Publishing Corporation, New York (1978).
38. Y. Chen, L. Jallo, M. A. S. Quintanilla and R. Dave, *Colloids Surface A* **361**, 66–80 (2010).
39. A. Busnaina, J. Taylor and I. Kashkoush, *J. Adhesion Sci. Technol*. **7**, 441–455 (1993).